Published in final edited form as:
Invest Ophthalmol Vis Sci. 2008 July ; 49(7): 3178–3184.

Ionic Dysregulatory Phenotyping of Pathologic Retinal Thinning with Manganese-Enhanced MRI

Bruce A. Berkowitz[1,2], **Marius Gradianu**[1], **Stephen Schafer**[1], **Ying Jin**[1], **Andre Porchia**[1], **Raymond Iezzi**[2], and **Robin Roberts**[1]

1*Department of Anatomy and Cell Biology, Wayne State University, Detroit, Michigan.*

2*Department of Ophthalmology, Wayne State University, Detroit, Michigan.*

Abstract

PURPOSE—To test the hypothesis that manganese-enhanced MRI (MEMRI) provides a sensitive and robust measure of an important retinal ionic dysregulatory phenotype in pathologic retinal thinning.

METHODS—Four hours after intraperitoneal $MnCl_2$ injection, high-resolution MEMRI data were collected from overnight dark-adapted male control Sprague–Dawley and albino Royal College of Surgeons rats before (at development stage postnatal day [P] 17) and during photoreceptor degeneration (P36 and P57). In separate experiments, control rats, with and without repetitive hypoxic preconditioning, were subjected to high IOP (100 mm Hg) for 60 minutes followed by 24 hours or 7 days of reperfusion (e.g., ischemia/reperfusion). Central retinal thickness and intraretinal ion activity were measured from the MEMRI data. Histology examination was also performed to confirm retinal damage.

RESULTS—In two different neurodegenerative models, MEMRI revealed first-time evidence for changes ($P < 0.05$) in intraretinal ion regulation before and during pathologic, but not ($P > 0.05$) developmental, retinal thinning. This phenotype was significantly altered by a neuroprotective repetitive hypoxic preconditioning protocol.

CONCLUSIONS—MEMRI and a nontoxic systemic dose of $MnCl_2$ provided an objective, noninvasive measure of an ionic deregulatory phenotype that appears useful for improved early diagnosis and treatment prognosis in a range of neurodegenerative diseases and their treatment.

There is no effective treatment for major neurodegenerative diseases of the visual system, such as retinitis pigmentosa (RP), though promising experimental therapies are being developed. Because neurodegeneration is irreversible, it is critical that diagnosis and prognosis of treatment efficacy be made as early as possible in the course of the disease. Electroretinography (ERG) is a leading method for assessing retinal health and has been used to measure functional changes before morphologic changes in experimental and clinical studies.[1] However, ERG measures an integrated response from whole retina, and this decreases its sensitivity to focal lesions. Multifocal electroretinographic methods address this concern but are not easily applied in small animal models. In addition, it is unclear how whole-retina ERG results and noninvasive morphology outcome metrics (i.e., ocular coherence tomography [OCT]), which are measured over a relatively much smaller region of retina, can be quantitatively compared. In addition,

Corresponding author: Bruce A. Berkowitz, Department of Anatomy and Cell Biology, Wayne State University School of Medicine, 540 E. Canfield, Detroit, MI 48201; baberko@med.wayne.edu.

Disclosure: **B.A. Berkowitz**, None; **M. Gradianu**, None; **S. Schafer**, None; **Y. Jin**, None; **A. Porchia**, None; **R. Iezzi**, None; **R. Roberts**, None

neither ERG nor OCT directly assesses postreceptoral (i.e., inner retina) and photoreceptoral (i.e., outer retina) metabolic alterations linked with neuronal loss. There is a pressing need for noninvasive methods that can identify, with high spatial resolution, a robust phenotype of retinal activity that is quantitatively sensitive to the extent of degeneration in experimental models in vivo.

Maintaining transmembrane ion gradients is essential for healthy neuronal function. Importantly, growing evidence supports a pathogenic role for early changes in intraretinal ion activity during a clinically silent phase first involving impaired ion handling and then an increased flux of ions such as calcium, which, in turn, likely triggers apoptosis and neuronal loss.[1–5] Furthermore, reducing flux through ion channels is neuroprotective against ischemic damage.[5,6] We reason that a noninvasive measurement of an ionic dysregulatory phenotype before and during the onset of retinal cell death would allow for early, and thus more rapid, testing of retinas at risk for degeneration and efficacy of new neuroprotective therapies.

Manganese-enhanced MRI (MEMRI) is a powerful, noninvasive, high-resolution approach for studying ionic regulation colocalized with structure and has been applied across disciplines such as cardiology, oncology, and neurology and includes the retina.[7–13] We, and others,[7,8,12–14] have validated that, after systemic injection of a nontoxic dose of $MnCl_2$, manganese (Mn^{2+}), an MRI contrast agent and ion analog of, for example, calcium, readily accumulates intracellularly as a function of membrane integrity and cellular activity and is relatively slowly removed. To date, MEMRI studies of retinal degeneration have not been reported.

In this study, we tested the hypothesis that MEMRI sensitively and robustly measures an ionic dysregulatory phenotype within the retina. To determine whether this pathologic phenotype represents a common defect not linked to a particular model or sex of the rat, two different degenerative models were studied using male or female Royal College of Surgeons (RCS) rats, a well-studied model with similarities to autosomal recessive retinitis pigmentosa.[15] In addition, a model of acutely induced ischemia/reperfusion (I/R) injury produced by elevated intraocular pressure (IOP) was investigated.[1] We also examined whether repetitive hypoxic (RH) preconditioning, a protocol that is neuroprotective, could alter ionic regulation within the retina.[16]

METHODS

The animals were treated in accordance with the National Institutes of Health Guide for the Care and Use of Laboratory Animals and the ARVO Statement for the Use of Animals in Ophthalmic and Vision Research. In all cases, rats (200–250 g) were housed and maintained in normal 12-hour light/12-hour dark cycling. The day before the MRI experiment, rats were placed and maintained in total darkness overnight. All procedures (e.g., weighing rat, injecting $MnCl_2$, anesthesia for MRI, and MRI examination) were performed in the presence of dim red light or darkness. $MnCl_2$ was administered as an intraperitoneal injection (44 mg/kg) to awake rats. These rats were maintained awake in dark conditions for another 3.5 hours, then anesthetized and imaged (MEMRI study) or killed for the toxicity study.

Control and Dystrophic Retinal Thinning Groups

Male albino control Sprague–Dawley and albino RCS (breeders provided by Matthew LaVail) rats were examined with MEMRI at three time points. These times in the RCS rat represent the following three key points in the course of neurodegeneration: before gross photoreceptor changes (postnatal day [P] 17, $n = 4$ control and 6 RCS), after significant loss of rods (P36, $n = 5$ control and 8 RCS), and after substantial degeneration of cones (P57, $n = 5$ control and 6 RCS).[17] Although recent data suggest that it is reasonable to measure the evolution of ion regulation in the same rat after a single intraperitoneal bolus of manganese, these data were

available only after the experiments performed herein, and so only new groups of rats were studied at each time point.[14] Additional experiments are needed to determine whether periodic exposure to subtoxic manganese levels are associated with histologic or physiological damage to the retina. After the P57 MEMRI examination, rats were killed for histologic examination.

Repetitive Hypoxia and Elevated Intraocular Pressure

Four groups of female Sprague–Dawley albino rats were studied: a nonischemic room air control group ($n = 4$), a nonischemic RH preconditioned control group ($n = 4$), an I/R group ($n = 6$), and an I/R group pretreated with repetitive hypoxia (RH+I/R; $n = 4$). RH procedures consisted of exposing caged rats to 11% oxygen in a modified incubator in which the oxygen levels were controlled by a computer (Oxycycler; BioSpherix, Ltd., Redfield, NY) for 2 hours every other day for a total of 3 exposure days. The percentage of oxygen within each incubator was validated using a separate, calibrated, handheld sensor. To induce ischemia, elevated IOP was produced in room air or RH animals 4 days after the last hypoxic episode. Rats were first anesthetized with intraperitoneal injections of ketamine (60 mg/kg) and xylazine (6 mg/kg). The anterior chamber of one eye was cannulated with a 30-gauge needle attached to a line connected to a saline bag and a calibrated pressure transducer at rat eye level. The saline bag was raised to a height that produced a pressure in the eye of 100 mg. The duration of ischemia was 60 minutes. After the saline bag was lowered and normalization of IOP was confirmed, the needle was withdrawn and retinal reperfusion was visually confirmed. Animals were studied by MEMRI at either 24 hours or 7 days after ischemia. After the 7-day MEMRI examination, rats were killed for histologic examination.

Histology

After initial fixation in formalin overnight at 4°C, eyecups were post-fixed for 3 hours on ice in 0.67% osmium tetroxide and 0.83% glutaraldehyde in 0.1 M sodium phosphate buffer (pH 7.4). The eyecups were then rinsed with 0.1 M phosphate buffer, dehydrated in graded ethanols and propylene oxide, and embedded in Epon araldite. Semithick (1.5-mm) radial sections through the optic nerve head were cut with a ultramicrotome (Reichert-Jung Ultracut E; Cambridge Instruments, Buffalo, NY), contrasted with Richardson stain, and coverslipped for histopathologic evaluation of retinal layer thickness.

MEMRI

Immediately before the MRI experiment, rats were anesthetized intraperitoneally using urethane (36% solution, 0.083 mL/20 g animal weight, prepared fresh daily; Aldrich, Milwaukee, WI). To maintain the core temperature, a recirculating heated water blanket was used. Rectal temperatures were continuously monitored throughout each experiment, as previously described.[18] MRI data were acquired on a 4.7-T Bruker Avance system using a two-turn transmit/receive surface coil (1-cm diameter) placed over the eye. Images were acquired using an adiabatic spin-echo imaging sequence (repetition time, 350 seconds; echo time, 16.7 ms; number of acquisitions, 16; matrix size, 512 × 512; slice thickness, 620 μm; field of view, 12 × 12 mm^2; 54 minutes/image).[19] A single transverse slice through the center of the eye (based on sagittal localizer images collected using the same adiabatic pulse sequence, as described) was obtained for each rat.

Data Analysis

Retinal Thickness—Whole retinal thicknesses were measured from each MRI-generated image as the radial distance between the anterior edge and the posterior edge of the retina at distances ±0.4 to 1 mm from the optic nerve, as previously described and as validated against histology, on each image.[12] Mean superior and inferior values were generated for each rat and used for comparisons. No difference ($P > 0.05$) in whole retinal thickness were found between

the present data and our previous report in control female Sprague–Dawley rats; therefore, these data were combined.

Retinal Signal Intensities—Signal intensities of inner and outer retina were analyzed from 1 pixel-thick central retina (±0.4–1 mm from the optic nerve). For quantitative analysis, intraretinal signal intensities were analyzed using the program NIH IMAGE and derived macros.[20] Changes in receiver gain between animals were controlled by setting the signal intensity of a fixed region of noise in each rat to a fixed value. In retinas from control and RCS rats, a 1 pixel-thick line (representing the border between inner and outer retina) was set at 4 pixels (or approximately 94 μm) posterior to the clearly defined vitreoretinal division. Another 1 pixel-thick line was set at 3 pixels (or approximately 70 μm) posterior from this inner/outer division. Pixels immediately anterior to each line were considered representative of inner and outer retina, respectively, and were analyzed as previously described.[12] These retinal regions analyzed are also indicated here (see Fig. 2› Fig. 3). In the RCS rats, comparison of retinal signal intensity with histology obtained at P57 revealed that the debris layer (a characteristic lesion of the RCS phenotype in which the subretinal space fills with shed photoreceptor outer segments) also accumulated manganese (data not shown). Thus, in RCS rats, the thickness measured on MEMRI included this debris zone despite the fact that that the neurosensory retinal thickness was significantly lower than that in age-matched controls. In other words, “retinal” thickness measured from MEMRI of older RCS rats likely overestimated the retinal thickness. In the elevated IOP model, approximately 50% of the inner retina degenerates by 7 days after ischemia; no gross degeneration is noted by 24 hours after ischemia.[1,16,21–23] In this case, a 1 pixel-thick line was set 2 pixels (or approximately 47 μm) anterior to the well-defined scleroretinal border. Another 1-pixel line was drawn anteriorly by 3 pixels. As described, pixels immediately anterior to each line were considered representative of inner and outer retina, respectively, and were analyzed as previously described.[12] Images collected with the present parameters, from rats that were not injected with $MnCl_2$, had retinal signal intensities lower than 50 arbitrary units (data not shown). Thus, only retinas with intensities greater than 50 were included in the final intensity analysis, though, as mentioned, whole retinal thicknesses were measured from all retinas.

Statistical Analysis—Retinal thicknesses were consistent with a normal distribution, and comparisons between groups were mostly performed using an unpaired 2-tailed *t*-test or a Mann–Whitney *U* test (depending on the numbers of animals in a group). Because we hypothesized that I/R would reduce retinal thickness and that RH would improve retinal thickness, comparisons were performed using a 1-tailed test. Comparison of retinal signal intensities and Mn^{2+} ion enhancements were performed using a generalized estimating equation approach.[24] This method performed a general linear regression analysis using all the pixels from each subject and accounts for the within-subject correlation between adjacent pixels. In all cases, unless otherwise noted, 2-tailed $P < 0.05$ was considered significant.

RESULTS

Constant Intraretinal Ionic Regulation during Developmental Thinning

During maturation in rodents, retinal thinning continues after differentiation.[25,26] MEMRI could readily measure ($P < 0.05$) this retinal thinning between P17 (258.7 ± 4.1 μm; $n = 4$; mean ± SEM) and P57 (197.1 ± 2.5 μm; $n = 5$; Fig. 1). During developmental thinning, a constant extent of manganese uptake in inner and outer retina was measured (Fig. 2).

Identification of an Ionic Dysregulatory Phenotype during Degeneration

RCS rats also demonstrated age-dependent retinal thinning, though by P57, the retina thickness (173.1 ± 2.9 μm; $n = 6$) was significantly thinner ($P < 0.05$) than that of age-matched controls

(197.1 ± 2.5 μm; $n = 5$; Fig. 1). Importantly, at P17, when there was little photoreceptor degeneration, retinawide manganese uptake in the RCS rat was subnormal and increased by P57 (Fig. 2). In addition, in P17 RCS rats, MEMRI detected a significant difference ($P < 0.05$) in the mean ratio of manganese uptake in inner and outer retina (9%; Fig. 2) compared with previously published ratios in light-adapted (1%) and dark-adapted (19%) control rats.[12]

Ionic Dysregulatory Phenotype in a Different Model of Degeneration

To test whether the ionic dysregulatory phenotype was a common defect linked with degeneration and not to a particular model or sex, we also examined a nondevelopmental, acute model of retinal degeneration using an established I/R IOP model applied to Sprague–Dawley adult female rats. At 24 hours after reperfusion, retinal thickness (193.4 ± 3.0 μm; $n = 4$) was not lower than control values (191.5 ± 1.1 μm; $n = 9$; $P > 0.05$). However, by 7 days, there was a significant ($P < 0.05$) decrease in total retinal thickness (161.5 ± 2.4 μm; $n = 6$) compared with that of controls. At 24 hours after I/R, retinawide manganese uptake was subnormal and increased between 1 and 7 days of I/R (Fig. 3).

Preconditioning Using Acute Hypoxia Attenuates I/R-Induced Decrease of Total Retinal Thickness

By 7 days after I/R, rats pretreated with repetitive hypoxia (RH+I/R) had less ($P < 0.05$) evidence of intraretinal damage and retinal thinning (173.9 ± 4.9 mm; $n = 4$) than those not preconditioned (I/R; 161.5 ± 2.4 μm; $n = 6$; Fig. 4). Note that compared with retinal thickness in control rats (191.5 ± 1.1 μm; $n = 9$), no evidence for hypoxia-induced retinal swelling was found on MEMRI (186.1 ± 5.2 μm; $n = 5$) examination ($P > 0.05$). Subnormal intraretinal manganese uptake after ischemia (RH+I/R) was also noted (Fig. 4). This subnormal response was likely caused by the RH procedure because control rats exposed to the same RH protocol also demonstrated subnormal uptake on MEMRI examination 7 days later (Fig. 4).

DISCUSSION

In this study, we identified a central intraretinal ionic dysregulatory phenotype that occurred during pathologic, but not developmental, retinal thinning in which a significant predegenerative subnormal uptake of manganese was followed by an increase in the extent of uptake. In both models, changes in manganese uptake were not localized to the portion of retina involved with degeneration but instead were found throughout the retina. These observations support and expand our previous report of a panretinal change in manganese uptake after an injury localized to the retinal pigment epithelium.[14] Intriguingly, in all cases examined to date, such intraretinal spatial mirroring occurred before histologic evidence of degeneration. We speculate that early intraretinal changes reflected physiological upstream/downstream consequences of a focal injury. Furthermore, our data reveal that repetitive hypoxic preconditioning, a protocol that had previously only been tested in a murine I/R model,[16] is also neuroprotective in a rat I/R model. Importantly, RH significantly suppressed the ionic dysregulatory phenotype linked with degeneration. When considered together, the present data highlight for the first time the sensitivity of MEMRI to important retinawide changes in ion regulation in response to injury. One limitation of the MEMRI experiment is that it measures the end result of manganese accumulation in a particular retinal layer but cannot distinguish intracellular from extracellular location. Nonetheless, MEMRI appears to be a powerful, objective, and noninvasive approach that may improve early diagnosis and treatment prognosis in a range of neurodegenerative diseases.

Because high levels of manganese ion are generally considered toxic, it is worthwhile reviewing why the dose and route of administration of $MnCl_2$ used in the present study are not expected to adversely affect retinal anatomy or function. At our standard $MnCl_2$ dose (44 mg/

kg, intraperitoneally), no evidence for perturbed electroretinographic parameters was found at either 4 hours or 7 days after injection compared with control rats.[14] In addition, at 30 days after injection, whole and inner retinal thickness, IOP, and blood retinal barrier permeability surface area product were not different from those of control rats.[12] We also found that reinjection of the same group of control rats with $MnCl_2$, when retinal signal intensity had returned to baseline levels (≥1 week), yielded no significant difference in intraretinal uptake.[14] Importantly, we have validated that intraretinal manganese uptake reflects normal changes in the regulation of ion activity induced by, for example, light adaptation, Na^+K^+ ATPase activity, and L-type calcium channels.[7,12,14] Thus, it is reasonable to consider the use of a modest dose of $MnCl_2$ as nontoxic and the intraretinal uptake of manganese as a quantitative biomarker of ion activity regulation in vivo.

Apoptosis is a key factor in refinement of the mammalian retina during maturation and during retinal degeneration, though different molecular pathways appear to be involved.[27–29] For example, the upregulation of caspases plays a key role during developmental retinal cell death but not during degenerative photoreceptor death in certain in vivo models.[29] Despite strong evidence for ionic regulation of apoptosis,[24,30] the possibility of a differential degree of ionic regulation in development and degeneration is less clear. Our results suggest that transmembrane gradients are distinctly regulated during normal retinal maturation and abnormal retinal degeneration. More work is now needed to further understand the implications of these results.

In this study, a dystrophic rat model relevant to progressive degenerative disease in human eyes was studied. A hallmark of retinitis pigmentosa, a family of inherited disorders, is the loss of photoreceptor or retinal pigment epithelial function leading to progressive night blindness, reduction or loss of visual acuity, and gradual loss of the visual field. In the male RCS rats studied herein, we found evidence of impaired ion regulation at P17 (Fig. 2) that preceded the onset of major photoreceptor damage and, thus, did not seem to be a consequence of degeneration. Other evidence for perturbed ion regulation in RCS rats includes subnormal rhodopsin dephosphorylation kinetics that suppresses ion channel opening, leading to an extended light adaptation state even after overnight dark adaptation,[2,3] dysfunctional dopaminergic regulation, which may modulate Na^+K^+ ATPase activity,[31,32] abnormal uptake of an ion channel-permeant histology marker,[4] and significant changes in ionotropic and metabotropic receptors, two classes of postreceptor ion channel modulators.[17,33–36] Furthermore, the subsequent increase in intraretinal manganese uptake is in line with current evidence of channel opening leading to calcium overload, apoptosis, and photoreceptor demise.[1,2,5,37–40]

We also investigated another model of retinal degeneration in which female Sprague–Dawley rats were subjected to high IOP inducing global retinal ischemia, followed by different periods of reperfusion. In such a model, functional changes on ERG are detected 2 days after ischemia, but significant whole retinal thinning is only found later in the reperfusion period.[1,16,22,23] In the present IOP study, ketamine was used as an anesthetic. Ketamine attenuates NMDA receptor–induced neuronal cell death and is generally thought to be neuroprotective. Despite this potential confounder, the present data, and those of others, clearly demonstrate a benefit of preconditioning in ketamine-anesthetized I/R models (Fig. 4).[41,42] In the I/R model, subnormal uptake of manganese 1 day after ischemia (Fig. 3) appears consistent with early ischemia-induced impairment of the Na^+/K^+-ATPase pump and membrane depolarization, whereas subsequent increases in manganese uptake may be the result of channel opening and accumulation of sodium and calcium ions in the cytosol.[1,14,43] In both models examined (RCS and I/R), a similar late-stage uptake of manganese was found between controls and experimental rats, though it was not determined whether this was caused by a reestablishment of ionic homeostasis after degeneration or whether MEMRI studies at later times would have

revealed progressively higher manganese uptake. Nonetheless, when both models are considered, a similar early-phase ionic dysregulatory phenotype was found that appeared independent of the model of degeneration and sex of the cohort studied.

To examine the possible importance of this ionic dysregulatory phenotype to histopathologic outcome, I/R experiments were repeated with an RH preconditioning protocol that was reported to induce long-lasting neuroprotection in mice.[16] The effectiveness of RH in rats had not been previously examined. The data in Figure 4 support the notion that RH is effective in protecting the rat retina from ischemic injury. Furthermore, the data in Figure 4 are consistent with the triggering of an adaptive response by RH involving the downregulation of basal ion activity and thus lower intraretinal uptake of manganese. We speculate that such downregulation, in turn, reduced ionic overload during reperfusion and resulted in a reduction of injury (i.e., retinal thickness).[6] These data underscore the sensitivity of MEMRI because modification of the intraretinal ionic dysregulatory phenotype in a manner consistent with neuroprotective mechanisms could be readily measured.

Before the present study, it was not possible to noninvasively and simultaneously monitor the spatial and temporal changes in retinal layer-specific ion activity and thickness in any animal model of retinal degeneration in vivo. Based on the present data, MEMRI examination of retina degeneration is likely to be widely applicable for the rapid development of new and useful treatment strategies for a range of neurodegenerative disease.

Acknowledgments

The authors thank Dennis Goebel and Jeff Gidday for helpful comments.

Supported by National Institutes of Health Grant EY010221, the Juvenile Diabetes Research Foundation, and an unrestricted grant from Research to Prevent Blindness. Histology service was provided by a Core Grant for Vision Research (P30EY004068).

References

1. Osborne NN, Casson RJ, Wood JP, Chidlow G, Graham M, Melena J. Retinal ischemia: mechanisms of damage and potential therapeutic strategies. Prog Retin Eye Res 2004;23:91–147. [PubMed: 14766318]
2. Ohguro H, Ohguro I, Mamiya K, Maeda T, Nakazawa M. Prolonged survival of the phosphorylated form of rhodopsin during dark adaptation of Royal College Surgeons rat. FEBS Lett 2003;551:128–132. [PubMed: 12965217]
3. Perlman I. Dark-adaptation in abnormal (RCS) rats studied electroretinographically. J Physiol 1978;278:161–175. [PubMed: 671282]
4. Kalloniatis M, Tomisich G, Wellard JW, Foster LE. Mapping photoreceptor and postreceptoral labelling patterns using a channel permeable probe (agmatine) during development in the normal and RCS rat retina. Vis Neurosci 2002;19:61–70. [PubMed: 12180860]
5. Fox DA, Poblenz AT, He L, Harris JB, Medrano CJ. Pharmacological strategies to block rod photoreceptor apoptosis caused by calcium overload: a mechanistic target-site approach to neuroprotection. Eur J Ophthalmol 2003;13:S44–S56. [PubMed: 12749677]
6. Hochachka PW, Lutz PL. Mechanism, origin, and evolution of anoxia tolerance in animals. Comp Biochem Physiol B: Biochem Mol Biol 2001;130:435–459. [PubMed: 11691622]
7. Lu H, Xi ZX, Gitajn L, Rea W, Yang Y, Stein EA. Cocaine-induced brain activation detected by dynamic manganese-enhanced magnetic resonance imaging (MEMRI). Proc Natl Acad Sci U S A 2007;104:2489–2494. [PubMed: 17287361]
8. Wendland MF. Applications of manganese-enhanced magnetic resonance imaging (MEMRI) to imaging of the heart. NMR Biomed 2004;17:581–594. [PubMed: 15761947]

9. Chaudhri OB, Parkinson JRC, Kuo YT, et al. Differential hypothalamic neuronal activation following peripheral injection of GLP-1 and oxyntomodulin in mice detected by manganese-enhanced magnetic resonance imaging. Biochem Biophys Res Comm 2006;350:298–306. [PubMed: 17007819]
10. Skjold A, Kristoffersen A, Vangberg TR, Haraldseth O, Jynge P, Larsson HB. An apparent unidirectional influx constant for manganese as a measure of myocardial calcium channel activity. J Magn Reson Imaging 2006;24:1047–1055. [PubMed: 17024667]
11. Braun RD, Gradianu M, Vistisen KS, Roberts RL, Berkowitz BA. Manganese-enhanced MRI of human choroidal melanoma xenografts. Invest Ophthalmol Vis Sci 2007;48:963–967. [PubMed: 17325133]
12. Berkowitz BA, Roberts R, Goebel DJ, Luan H. Noninvasive and simultaneous imaging of layer-specific retinal functional adaptation by manganese-enhanced MRI. Invest Ophthalmol Vis Sci 2006;47:2668–2674. [PubMed: 16723485]
13. Lin YJ, Koretsky AP. Manganese ion enhances T1-weighted MRI during brain activation: an approach to direct imaging of brain function. Magn Reson Med 1997;38:378–388. [PubMed: 9339438]
14. Berkowitz BA, Roberts R, Luan H, et al. Manganese-enhanced MRI studies of alterations of intraretinal ion demand in models of ocular injury. Invest Ophthalmol Vis Sci 2007;48:3796–3804. [PubMed: 17652754]
15. Gal A, Li Y, Thompson DA, et al. Mutations in MERTK, the human orthologue of the RCS rat retinal dystrophy gene, cause retinitis pigmentosa. Nat Genet 2000;26:270–271. [PubMed: 11062461]
16. Zhu Y, Zhang Y, Ojwang BA, Brantley MA Jr, Gidday JM. Long-term tolerance to retinal ischemia by repetitive hypoxic preconditioning: role of HIF-1alpha and heme oxygenase-1. Invest Ophthalmol Vis Sci 2007;48:1735–1743. [PubMed: 17389506]
17. Fletcher EL, Kalloniatis M. Neurochemical architecture of the normal and degenerating rat retina. J Comp Neurol 1996;376:343–360. [PubMed: 8956104]
18. Berkowitz BA, Ito Y, Kern TS, McDonald C, Hawkins R. Correction of early subnormal superior hemiretinal ΔPO(2) predicts therapeutic efficacy in experimental diabetic retinopathy. Invest Ophthalmol Vis Sci 2001;42:2964–2969. [PubMed: 11687543]
19. Schupp DG, Merkle H, Ellermann JM, Ke Y, Garwood M. Localized detection of glioma glycolysis using edited 1H MRS. Magn Reson Med 1993;30:18–27. [PubMed: 8371670]
20. Berkowitz BA. Adult and newborn rat inner retinal oxygenation during carbogen and 100% oxygen breathing: comparison using magnetic resonance imaging ΔPO(2) mapping. Invest Ophthalmol Vis Sci 1996;37:2089–2098. [PubMed: 8814148]
21. Liu Q, Ju WK, Crowston JG, et al. Oxidative stress is an early event in hydrostatic pressure induced retinal ganglion cell damage. Invest Ophthalmol Vis Sci 2007;48:4580–4589. [PubMed: 17898281]
22. Roth S. Endogenous neuroprotection in the retina. Brain Res Bull 2004;62:461–466. [PubMed: 15036558]
23. Rosenbaum DM, Rosenbaum PS, Singh M, et al. Functional and morphologic comparison of two methods to produce transient retinal ischemia in the rat. J Neuroophthalmol 2001;21:62–68. [PubMed: 11315985]
24. Yu SP, Canzoniero LMT, Choi DW. Ion homeostasis and apoptosis. Curr Opin Cell Biol 2001;13:405–411. [PubMed: 11454444]
25. Braekevelt CR, Hollenberg MJ. The development of the retina of the albino rat. Am J Anat 1970;127:281–301. [PubMed: 5436824]
26. Young RW. Cell death during differentiation of the retina in the mouse. J Comp Neurol 1984;229:362–373. [PubMed: 6501608]
27. Hsu CD, Whaley MA, Frazer K, et al. limited role of developmental programmed cell death pathways in *Drosophila* norpA retinal degeneration. J Neurosci 2004;24:500–507. [PubMed: 14724249]
28. Bahi N, Zhang J, Llovera M, Ballester M, Comella JX, Sanchis D. Switch from caspase-dependent to caspase-independent death during heart development: essential role of endonuclease G in ischemia-induced DNA processing of differentiated cardiomyocytes. J Biol Chem 2006;281:22943–22952. [PubMed: 16754658]
29. Doonan F, Donovan M, Gomez-Vicente V, Bouillet P, Cotter TG. Bim expression indicates the pathway to retinal cell death in development and degeneration. J Neurosci 2007;27:10887–10894. [PubMed: 17913922]

30. Yu SP. Regulation and critical role of potassium homeostasis in apoptosis. Prog Neurobiol 2003;70:363–386. [PubMed: 12963093]

31. Djamgoz MB, Hankins MW, Hirano J, Archer SN. Neurobiology of retinal dopamine in relation to degenerative states of the tissue. Vision Res 1997;37:3509–3529. [PubMed: 9425527]

32. Shulman LM, Fox DA. Dopamine inhibits mammalian photoreceptor Na+,K+-ATPase activity via a selective effect on the α3 isozyme. Proc Natl Acad Sci U S A 1996;93:8034–8039. [PubMed: 8755598]

33. Cuenca N, Pinilla I, Sauve Y, Lund R. Early changes in synaptic connectivity following progressive photoreceptor degeneration in RCS rats. Eur J Neurosci 2005;22:1057–1072. [PubMed: 16176347]

34. Fletcher EL, Kalloniatis M. Neurochemical development of the degenerating rat retina. J Comp Neurol 1997;388:1–22. [PubMed: 9364235]

35. Stasi K, Naskar R, Thanos S, Kouvelas ED, Mitsacos A. Benzodiazepine and kainate receptor binding sites in the RCS rat retina. Graefes Arch Clin Exp Ophthalmol 2003;241:154–160. [PubMed: 12605271]

36. Armata IA, Giompres P, Smith A, Stasi K, Kouvelas ED, Mitsacos A. Genetically induced retinal degeneration leads to changes in metabotropic glutamate receptor expression. Neurosci Lett 2006;393:12–17. [PubMed: 16213654]

37. Tso MO, Zhang C, Abler AS, et al. Apoptosis leads to photoreceptor degeneration in inherited retinal dystrophy of RCS rats. Invest Ophthalmol Vis Sci 1994;35:2693–2699. [PubMed: 8188463]

38. Katai N, Kikuchi T, Shibuki H, et al. Caspaselike proteases activated in apoptotic photoreceptors of Royal College of Surgeons rats. Invest Ophthalmol Vis Sci 1999;40:1802–1886. [PubMed: 10393051]

39. Sharma AK, Rohrer B. Sustained elevation of intracellular cGMP causes oxidative stress triggering calpain-mediated apoptosis in photoreceptor degeneration. Curr Eye Res 2007;32:259–269. [PubMed: 17453946]

40. Traverso V, Bush RA, Sieving PA, Deretic D. Retinal cAMP levels during the progression of retinal degeneration in rhodopsin P23H and S334ter transgenic rats. Invest Ophthalmol Vis Sci 2002;43:1655–1661. [PubMed: 11980887]

41. Roth S, Li B, Rosenbaum PS, et al. Preconditioning provides complete protection against retinal ischemic injury in rats. Invest Ophthalmol Vis Sci 1998;39:777–785. [PubMed: 9538885]

42. Ranchon CI, Bonhomme B, Doly M. Pre-treatment of adult rats with high doses of erythropoietin induces caspase-9 but prevents light-induced retinal injury. Exp Eye Res 2007;85:782–789. [PubMed: 17961554]

43. Kuboki J, Ishiguro S, Tamai M. Susceptibility of weakly ouabain-sensitive Na,K-ATPase isoform in ischemic and reperfused rat retinas. Tohoku J Exp Med 1999;187:353–361. [PubMed: 10503607]

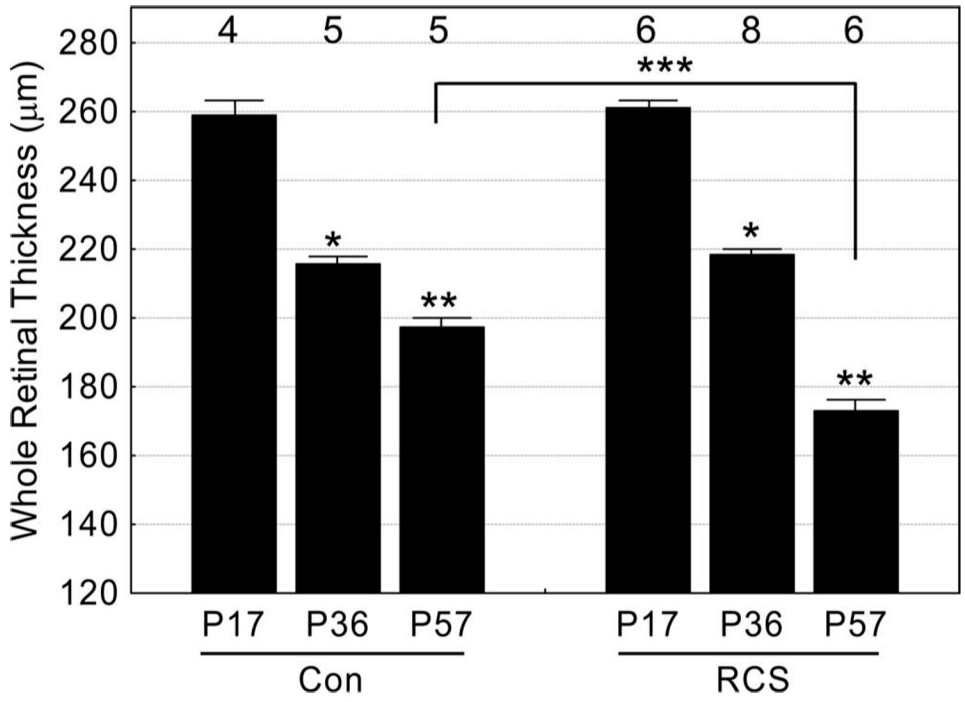

FIGURE 1.

Total retinal thickness measurements for male RCS rats at three time points: before (at developmental stage P17) and during (P36 and P57) photoreceptor degeneration. Age-matched control (con) rats were also studied. Numbers of animals used to generate these data are listed above bars. Error bars represent SEM. Brackets represent between-group comparisons with $P < 0.05$. *Significant differences from P17 data. **Significant differences from P17 and P36 data. ***Significant differences between P57 groups.

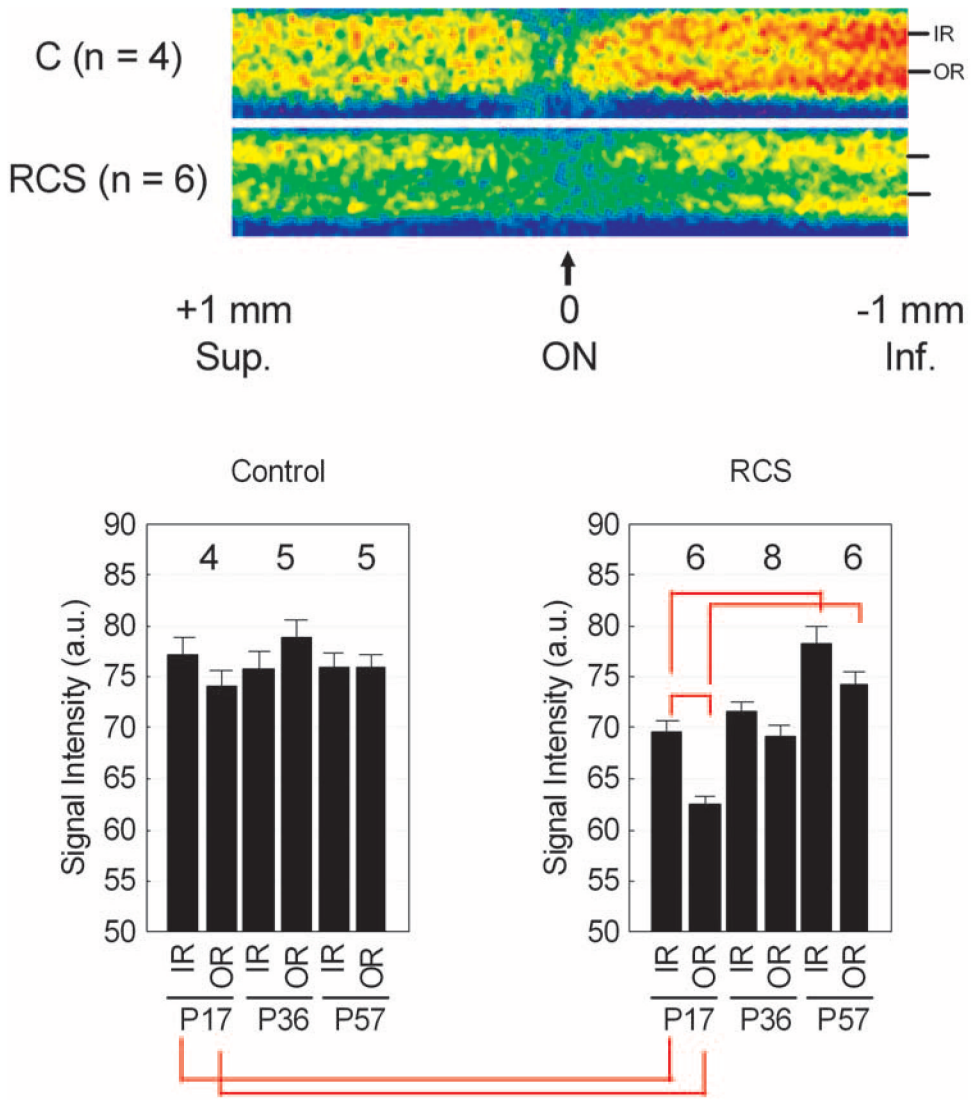

FIGURE 2.

Summary of changes in MEMRI intraretinal signal intensity during development and degeneration. *Top*: pseudocolor linearized images of average retinal signal intensity in central retina of P17 dark-adapted control male Sprague–Dawley rats (*top*, C; $n = 4$) and RCS (*bottom;* $n = 6$). The same pseudocolor scale was used for both linearized images, where *blue* to *green* to *yellow* to *red* represent lowest to highest signal intensity. The intraretinal location used to extract inner retinal (IR) and outer retinal (OR) data used in this study are indicated on the right of each linearized image. The scale on the bottom indicates the location of the optic nerve (ON) and the superior and inferior directions. *Bottom*: summary of inner and outer retinal signal intensities over time for control (*left*) and RCS (*right*) rats. *Red brackets*: between-group comparisons with $P < 0.05$. Error bars are SEM, and numbers above bars are numbers of animals studied.

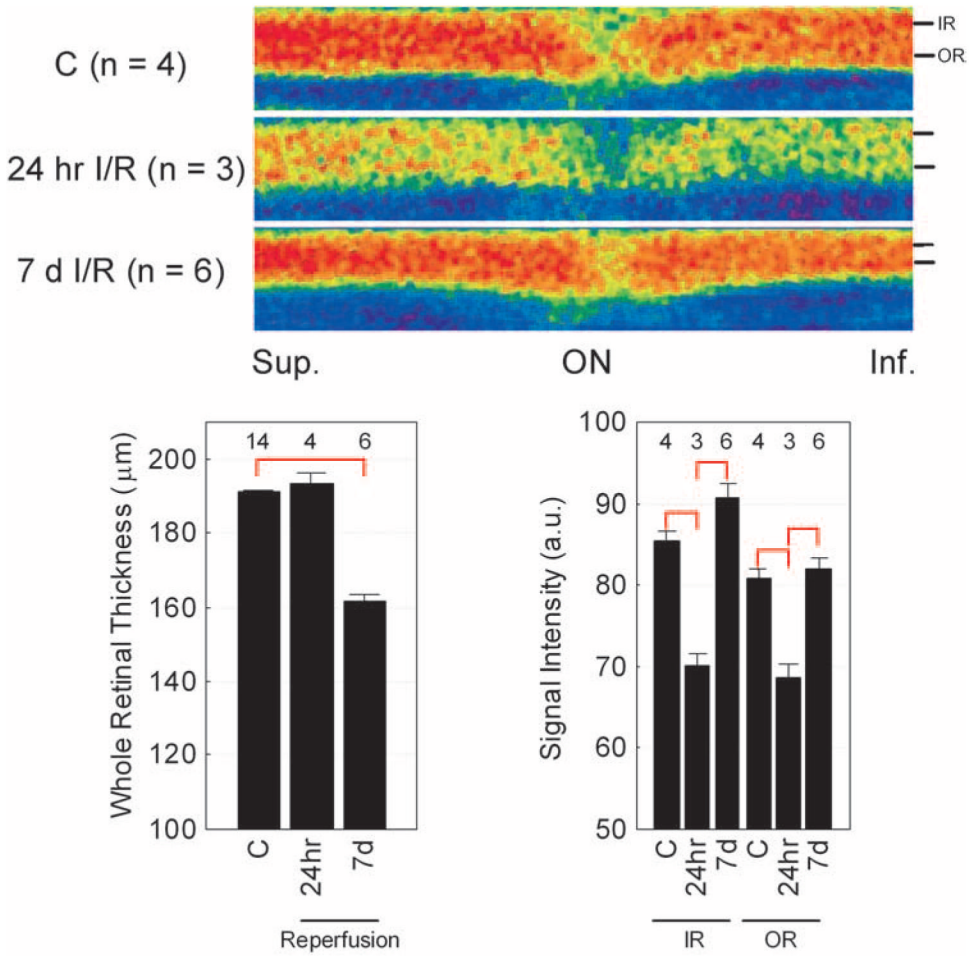

FIGURE 3.

Summary of changes in MEMRI intraretinal signal intensity in I/R. *Top*: pseudocolor linearized images of average retinal signal intensity in central retina of dark-adapted control female Sprague–Dawley rats (*top*, C; $n = 4$) after 24 hours of reperfusion (*middle*, 24-hour I/R; $n = 3$) and 7 days of reperfusion (*bottom*, 7 d I/R; $n = 6$). The same pseudocolor scale was used for both linearized images, where *blue* to *green* to *yellow* to *red* represent lowest to highest signal intensity. The intraretinal location used to extract inner (IR) and outer (OR) retinal data used in this study is indicated on the right of each linearized image. The scale on the bottom indicates the location of the optic nerve (ON) and superior and inferior directions. *Bottom*: summary of temporal evolution of whole retinal thickness (*left*) and inner (IR) and outer (OR) retinal signal intensities. *Red brackets*: between-group comparisons, with $P < 0.05$. Error bars represent SEM, and numbers over bars are numbers of animals studied.

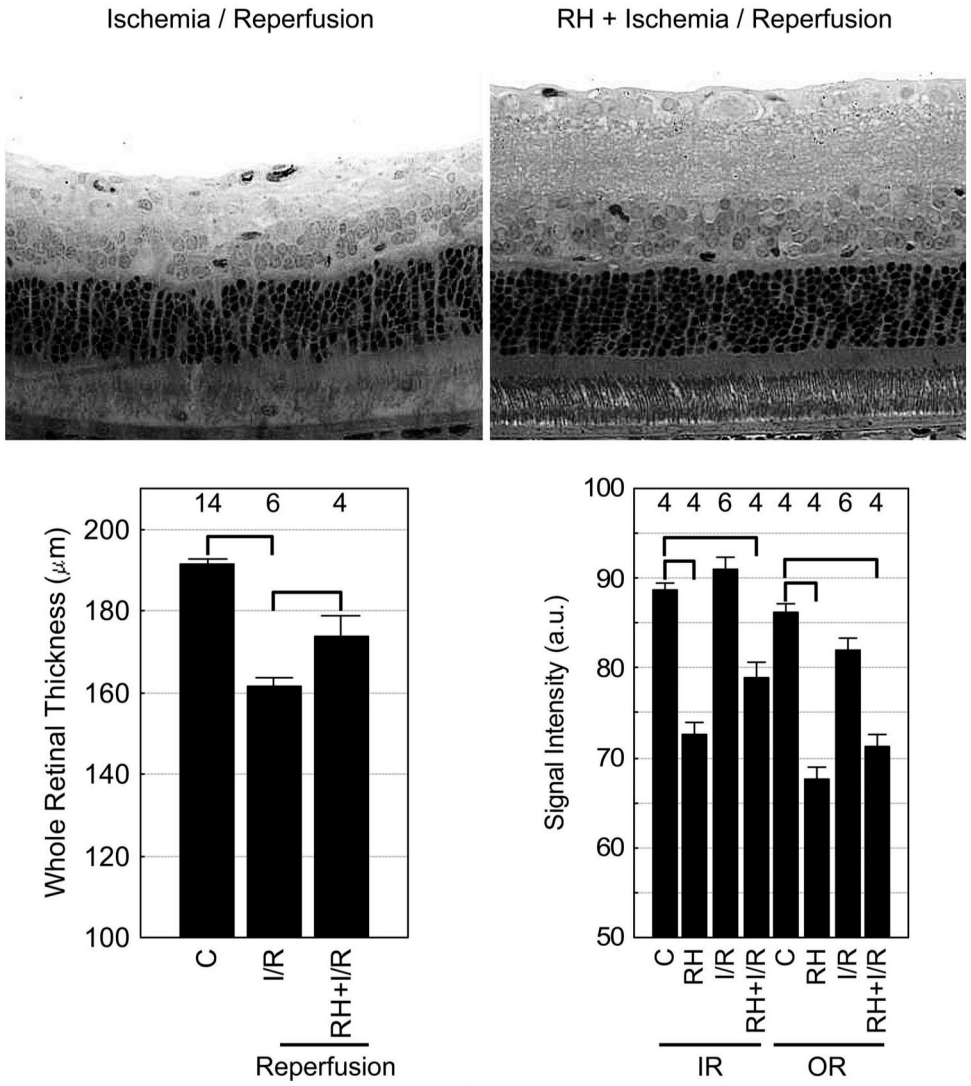

FIGURE 4.

Summary of the effect of repetitive hypoxic preconditioning on MEMRI signal intensity in I/R. *Top*: representative retinal histology after I/R (*left*) and RH+I/R (*right*) in female Sprague–Dawley rats collected under the same magnification. One week after ischemia, samples were collected immediately after MEMRI examination. To optimize the visual display of these data, both images were digitally sharpened by the same extent and contrast enhanced automatically based on the signal histogram. These procedures ensured that subjective bias was not introduced. *Bottom*: whole retinal thickness (*left*) measured from MEMRI data from control (C) rats, rats that had undergone ischemia and 7 days of reperfusion (I/R), or rats that had first been preconditioned (RH) and then subjected to ischemia and reperfusion (RH+I/R). Inner retinal (IR) and outer retinal (OR) signal intensities (*right*) from each group. *Brackets*: between-group comparisons with $P < 0.05$. Error bars represent SEM, and numbers over bars are numbers of animals studied. Note the untreated 7-day I/R data are reproduced from Figure 3 to aid comparison.